NASA/TM—2017-219715

Thermophysical Properties of Cold and Vacuum Plasma Sprayed Cu-Cr-X Alloys, NiAl and NiCrAlY Coatings

Part 1: Electrical and Thermal Conductivity, Thermal Diffusivity, and Total Hemispherical Emissivity

S.V. Raj
Glenn Research Center, Cleveland, Ohio

November 2017

NASA STI Program . . . in Profile

Since its founding, NASA has been dedicated to the advancement of aeronautics and space science. The NASA Scientific and Technical Information (STI) Program plays a key part in helping NASA maintain this important role.

The NASA STI Program operates under the auspices of the Agency Chief Information Officer. It collects, organizes, provides for archiving, and disseminates NASA's STI. The NASA STI Program provides access to the NASA Technical Report Server—Registered (NTRS Reg) and NASA Technical Report Server—Public (NTRS) thus providing one of the largest collections of aeronautical and space science STI in the world. Results are published in both non-NASA channels and by NASA in the NASA STI Report Series, which includes the following report types:

- TECHNICAL PUBLICATION. Reports of completed research or a major significant phase of research that present the results of NASA programs and include extensive data or theoretical analysis. Includes compilations of significant scientific and technical data and information deemed to be of continuing reference value. NASA counter-part of peer-reviewed formal professional papers, but has less stringent limitations on manuscript length and extent of graphic presentations.

- TECHNICAL MEMORANDUM. Scientific and technical findings that are preliminary or of specialized interest, e.g., "quick-release" reports, working papers, and bibliographies that contain minimal annotation. Does not contain extensive analysis.

- CONTRACTOR REPORT. Scientific and technical findings by NASA-sponsored contractors and grantees.

- CONFERENCE PUBLICATION. Collected papers from scientific and technical conferences, symposia, seminars, or other meetings sponsored or co-sponsored by NASA.

- SPECIAL PUBLICATION. Scientific, technical, or historical information from NASA programs, projects, and missions, often concerned with subjects having substantial public interest.

- TECHNICAL TRANSLATION. English-language translations of foreign scientific and technical material pertinent to NASA's mission.

For more information about the NASA STI program, see the following:

- Access the NASA STI program home page at http://www.sti.nasa.gov

- E-mail your question to help@sti.nasa.gov

- Fax your question to the NASA STI Information Desk at 757-864-6500

- Telephone the NASA STI Information Desk at 757-864-9658

- Write to:
  NASA STI Program
  Mail Stop 148
  NASA Langley Research Center
  Hampton, VA 23681-2199

NASA/TM—2017-219715

Thermophysical Properties of Cold and Vacuum Plasma Sprayed Cu-Cr-X Alloys, NiAl and NiCrAlY Coatings

Part 1: Electrical and Thermal Conductivity, Thermal Diffusivity, and Total Hemispherical Emissivity

S.V. Raj
Glenn Research Center, Cleveland, Ohio

National Aeronautics and
Space Administration

Glenn Research Center
Cleveland, Ohio 44135

November 2017

Acknowledgments

The experimental measurements were conducted by the Thermophysical Properties Research Laboratory, Inc. (TPRL), West Lafayette, Indiana, under contract. Their contributions are gratefully acknowledged. The author also thanks his colleague, Dr. Dongming Zhu, for measuring the thermal conductivity of NiCrAlY (Figure 5) by the dynamic laser measurement method at the NASA Glenn Research Center, and for his comments and suggestions on this paper. This paper was pubished in the Journal of Engineering Materials and Performance and can be found at https://link.springer.com/article/10.1007/s11665-017-3012-0

Level of Review: This material has been technically reviewed by technical management.

Available from

NASA STI Program
Mail Stop 148
NASA Langley Research Center
Hampton, VA 23681-2199

National Technical Information Service
5285 Port Royal Road
Springfield, VA 22161
703-605-6000

This report is available in electronic form at http://www.sti.nasa.gov/ and http://ntrs.nasa.gov/

Thermophysical Properties of Cold and Vacuum Plasma Sprayed Cu-Cr-X Alloys, NiAl and NiCrAlY Coatings
Part 1: Electrical and Thermal Conductivity, Thermal Diffusivity, and Total Hemispherical Emissivity

S.V. Raj
National Aeronautics and Space Administration
Glenn Research Center
Cleveland, Ohio 44135

Abstract

This two-part paper reports the thermophysical properties of several cold and vacuum plasma sprayed monolithic Cu and Ni-based alloy coatings. Part I presents the electrical and thermal conductivity, thermal diffusivity, and total hemispherical emissivity data while Part II reports the specific heat capacity data for these coatings. Metallic copper alloys, stoichiometric NiAl and NiCrAlY coatings were fabricated by either the cold sprayed or the vacuum plasma spray deposition processes for thermal property measurements between 77 and 1223 K. The temperature dependencies of the thermal conductivities, thermal diffusivities, electrical conductivities and total hemispherical emissivities of these cold and vacuum sprayed monolithic coatings are reported in this paper. The electrical and thermal conductivity data correlate reasonably well for Cu-8%Cr-1%Al, Cu-23%Cr-5%Al and NiAl in accordance with the Wiedemann-Franz (WF) law although a better fit is obtained using the Smith-Palmer relationship. The Lorentz numbers determined from the WF law are close to the theoretical value.

1.0 Introduction

The availability of good quality thermophysical data is key for simulating the performance of engineering components, and formulating theoretical models to gain fundamental insights on material behavior. The necessity for generating high quality data is more critical for aerospace components especially when two or more different materials are bonded to each other as in the case of coatings deposited on substrates.

Combustion liner materials in a liquid hydrogen (LH_2) fueled rocket engine experience extreme conditions due to a combination of environmental and thermo-mechanical effects, where the combustion flame temperatures in the chamber interior are about 3600 K whereas the backside of the 1 mm thick liner wall experiences cryogenic temperatures of 20 K (Refs. 1 to 6). Copper and its alloys have been used as combustor liner materials in these regenerative rocket engines because of their high thermal conductivity to enable efficient heat transfer from the combustion flame to preheat the cryogenic LH_2 flowing in the cooling channels. The GRCop-84 (Cu-8(at.%)Cr-4%Nb) copper alloy is a potential candidate material to replace currently-used NARloy-Z copper alloy combustor liners in the next generation of reusable launch vehicles (RLVs) due to its superior properties (Refs. 7, 8, and 9). However, uncoated copper alloy liners undergo environmental degradation due to a combination of the spallation of the copper oxide scale and “blanching”, which consists of repeated oxidation of the copper matrix and subsequent reduction of the oxide scale (Ref. 6).The application of protective coatings on GRCop-84 and other copper alloy substrates can minimize or eliminate many of the problems experienced by uncoated liners and significantly extend their operational lives in RLVs. The use of protective coatings is likely to increase component reliability,

reduce depot maintenance turnaround times and lower operational cost for using RLVs. In addition, the use of a suitable top coat to act as a thermal barrier can allow the engine to run at higher temperatures with a corresponding increase in thermal efficiency. As a result, several types of ceramic (Refs. 1 and 5) and metallic (Refs. 10 to 16) coatings have been advocated as protective coatings for copper alloy liners. It was demonstrated that CuCrAl and NiCrAlY coatings deposited either by the cold spray (CS) or the vacuum plasma spray (VPS) techniques are potentially viable coatings for GRCop-84 combustion liners (Refs. 14, 17 to 21).

However, the use of protective coatings on a substrate results in the development of residual stresses whenever the coated component experiences significant variations in temperature, such as during processing and thermal cycling conditions, in actual service. Therefore, it is essential that realistic finite element analysis (FEA) be conducted to give credence to the viability of these coated liners during use in RLVs in order to predict the performance of these coatings and to gain insights on the nature and magnitudes of the residual stresses.

The reliability of these modeling analyses require the generation of high quality of thermophysical data in addition to mechanical properties data. However, thermophysical data for these sprayed coatings are either limited or nonexistent in the temperature range of interest for use in RLVs. Although thermal conductivity data of vacuum plasma sprayed NiCrAlY alloys (Refs. 22 to 25) and NiAl (Ref. 26) have been previously reported in the literature, these properties are sensitive to compositional and processing variables. Similarly, although the thermal conductivities of copper alloys have been reported in early investigations (Refs. 27 to 31), and more recently on the Cu-0.01 to 1.0 (at.%)Cr alloys (Ref. 32), there is virtually no data available on the CS and VPS copper alloys investigated in the present paper except for GRCop-84 (Refs. 7 and 9).Thus, it is essential that thermophysical data be generated on protective coatings sprayed under processing conditions and for compositions similar to those developed for spraying the GRCop-84 liners in order to ensure that the design models are reliable. Thermal expansion data for several VPS coatings investigated in the present study were reported earlier (Ref. 33), while the elastic moduli data for CS and VPS coatings were reported elsewhere (Ref. 34).The objectives of this two-part paper are to report the thermophysical data generated on CS and VPS Cu-Cr, CuCrAl, NiAl and NiCrAlY coating alloys as a function of absolute temperature, *T*, varying between 77 and 1223 K. Part I presents the electrical and thermal conductivity, thermal diffusivity, and total hemispherical emissivity data while Part II reports the specific heat capacity data for these coatings. It has been necessary to divide the papers in this manner due to the nature of the analyses of the data. For example, Part I presents electrical and thermal conductivity since they are related for metallic systems, whereas the analyses of the specific heat data in Part II are related to thermodynamic parameters.

2.0 Experimental Procedures

2.1 Alloy Composition and Processing

The nominal compositions of the alloy powders investigated in this research were Cu-8(wt.%)Cr, Cu-26(wt.%)Cr, Cu-8(wt.%)Cr-1%Al, Cu-23(wt.%)Cr-5%Al, Ni-31.5(wt.%)Al (NiAl), Ni-17(wt.%)Cr-6%Al-0.5%Y (NiCrAlY). Details of the powder suppliers and fabrication methods were reported earlier (Refs. 33, 34, and 35). Monolithic coatings,[1] typically 175 to 250 mm long and 19 to 25 mm thick, were fabricated by spraying the powders on rotating aluminum or steel mandrels by either the CS process or by

[1] The term “monolithic coatings” is used in a generic manner in this paper to distinguish cold and vacuum plasma sprayed powders from cast or extruded alloys.

the VPS method, respectively. The Cu-23%Cr-5%Al coatings were cold sprayed at ASB Industries, Inc., Barberton, Ohio (Refs. 17 and 35). The Cu-8%Cr, Cu-8%Cr-1%Al, NiAl and NiCrAlY coatings were deposited by the vacuum plasma spray method at Plasma Processes, Inc., Huntsville, Alabama (Ref. 33). The coated mandrels were hot isostatically pressed (HIP) between 1073 and 1273 K under argon gas pressures varying between 100 and 210 MPa for times varying between 1 and 4 hr. In addition, a Cu-17(wt.%)Cr-5%Al alloy was prepared by arc-melting the appropriate mixtures of Al, Cr and Cu chunks or pellets (Ref. 20). In this case, the button melt was flipped several times to homogenize the composition of the molten metal before being drop cast into a copper die cavity 12.7 mm diam. by 50 mm long. The alloy was homogenized annealed at 1223 K for 24 hr under flowing argon to minimize elemental segregation. Specimens were machined from the sprayed cylinders by electrodischarge machining (EDM). For baseline comparisons, density and thermophysical property measurements were also made on a hot-extruded GRCop-84 rod.

2.2 Thermophysical Property Measurements

The thermophysical property measurements reported in this paper were conducted at the Thermophysical Properties Research Laboratory, Inc. (TPRL), West Lafayette, Indiana, under contract. Details of the techniques for measuring several of the thermal properties reported in this paper are described elsewhere (Ref. 36). Table I gives the specimen dimensions for each thermal property measurement technique. The bulk density, ρ_d, of each specimen was calculated from its geometry and mass. High temperature thermal diffusivity, α, was measured between 295 and 1223 K under high vacuum using the laser flash techniques in accordance with ASTM E1461 (Ref. 37).The front face of the disc specimen was heated by a short laser burst from a Korad K2 laser apparatus and the resulting temperature rise at the back face was recorded and analyzed by a computerized system. Constant pressure specific heat, C_p, measurements on these monolithic coatings are reported in Part II (Ref. 38). The high temperature thermal conductivity, K_T, of the specimen was calculated from the relationship, $K_T = \alpha\rho_d C_p$. While the laser flash method of determining K_T is indirect, thermal conductivity of a NiCrAlY monolithic coating was also measured directly and dynamically using a laser beam of a known heat flux and measuring the front and back face temperatures on a 25.4 mm diam. by 3.1 mm thick disk specimen in order to compare the two sets of data. Details of this measurement technique are described elsewhere (Ref. 39).

Low temperature thermal conductivity, λ, and electrical resistivity, ρ, of the specimens were determined by the modified Kohlrausch method, which measures the product, $\lambda\rho$. The thermal conductivity measurements were conducted between 80 and 458 K in vacuum. Details of the technique and the methods used for separating λ and ρ from the measurements are described elsewhere (Ref. 36).

TABLE I.—DIMENSIONS OF SPECIMENS USED FOR DIFFERENT MEASUREMENTS[2]

Property	Measurement technique	Specimen dimensions, mm
Density	Mass and geometric volume	12.7 diam. by 1.5 to 5.0 thick (disk); 12.8 width by 12.8 width by 2.0 thick (square)
Electrical resistance/thermal conductivity (low temperature)	Kohlrausch method	88.9 long by 4.8 width by 2.5 thick
Total hemispherical emissivity	Heat balance (ASTM 835-06)	254 long by 4.8 width by 2.5 thick
Thermal conductivity/thermal diffusivity (high temperature)	Laser flash method (ASTM E1461)	12.7 diam. by 1.5 to 5.0 thick

[2] Measurements were conducted at Thermophysical Properties Research Laboratory, Inc., West Lafayette, Indiana.

Briefly, the method involves passing a direct current through the specimen to heat it while cooling the ends with liquid nitrogen. Radial heat losses were minimized by surrounding the specimen with an external heater with its center temperature maintained at the sample's midpoint temperatures. These test conditions ensured that a steady-state parabolic temperature profile was maintained along the axis of the specimen. Three thermocouples located at the specimen ends, designated as 1 and 3, and at its midpoint, designated as 2, were used as both voltage and temperature probes. Thus,

$$\lambda\rho = \frac{\left(V_3 - V_1\right)^2}{4\left[2T_2 - \left(T_1 + T_3\right)\right]} \tag{1}$$

$$\rho = \frac{\left(V_1 - V_3\right)A}{iL_{13}} \tag{2}$$

where V_j and T_j are voltages and absolute temperature readings from the j^{th} thermocouple (j = 1, 2 or 3), respectively, A is the specimen cross-sectional area, i is the current through the specimen and L_{13} is the distance between the end thermocouples, 1 and 3. The voltage and temperature data from the three thermocouples and the magnitudes of i were fed to a computerized data acquisition system, which enabled Equations (1) and (2) to be solved to evaluate λ and ρ for different sets of equilibrium conditions.

The total hemispherical emissivity, ε_H, was measured between 373 and 1223 K using a multi-property apparatus equipped with long vertical optical windows in accordance with ASTM 835-06 (Ref. 40). The specimen was mounted between two electrodes and heated under high vacuum by passing a direct current through it. The power dissipated over a small central region of the specimen was determined by measuring the product, $V \bullet i$, where V is the voltage, and the absolute temperature of the specimen midpoint, T_{mid}. In order to make measurements at the lower temperatures, the specimen was surrounded by a liquid nitrogen (LN_2)-cooled copper shield with its interior surface painted black. The magnitude of ε_H was calculated from

$$\varepsilon_H = \frac{V \bullet i}{P_c L \sigma \left(T_{mid}^4 - T_0^4\right)} \tag{3}$$

where P_c is the circumference of the specimen, L is the distance between voltage probes, σ is the Stefan-Boltzmann constant and T_0 is the ambient temperature.

3.0 Results and Discussion

3.1 Density and Microstructures

Table II shows the values of the bulk densities for several metallic monolithic coatings processed by different spraying techniques. The GRCop-84 and Cu-17%Cr-5%Al specimens were tested in the as-extruded and arc-melted conditions, respectively. The VPS Cu-26Cr (V2-02-27A) (Figure 1(a)) and VPS NiCrAlY (V2-02-27E) (Figure 1(b)) monolithic coatings had a significant amount of porosity and this fact is reflected in this batch having lower densities than material from batches V2-03-524 (VPS Cu-26%Cr) (Figure 1(c)) and V2-03-528 (VPS NiCrAlY) (Figure 1(d)), which were nearly 100% dense with little or no significant amount of porosity (Table I). The other coatings were close to 100% dense (Figure 1(e)). It is noted that the microstructures of VPS Cu-8%Cr, Cu-26%Cr and Cu-8%Cr-1%Al are similar with a distribution of α-Cr precipitates in either an α-Cu or α-(Cu,Al) matrix, respectively,

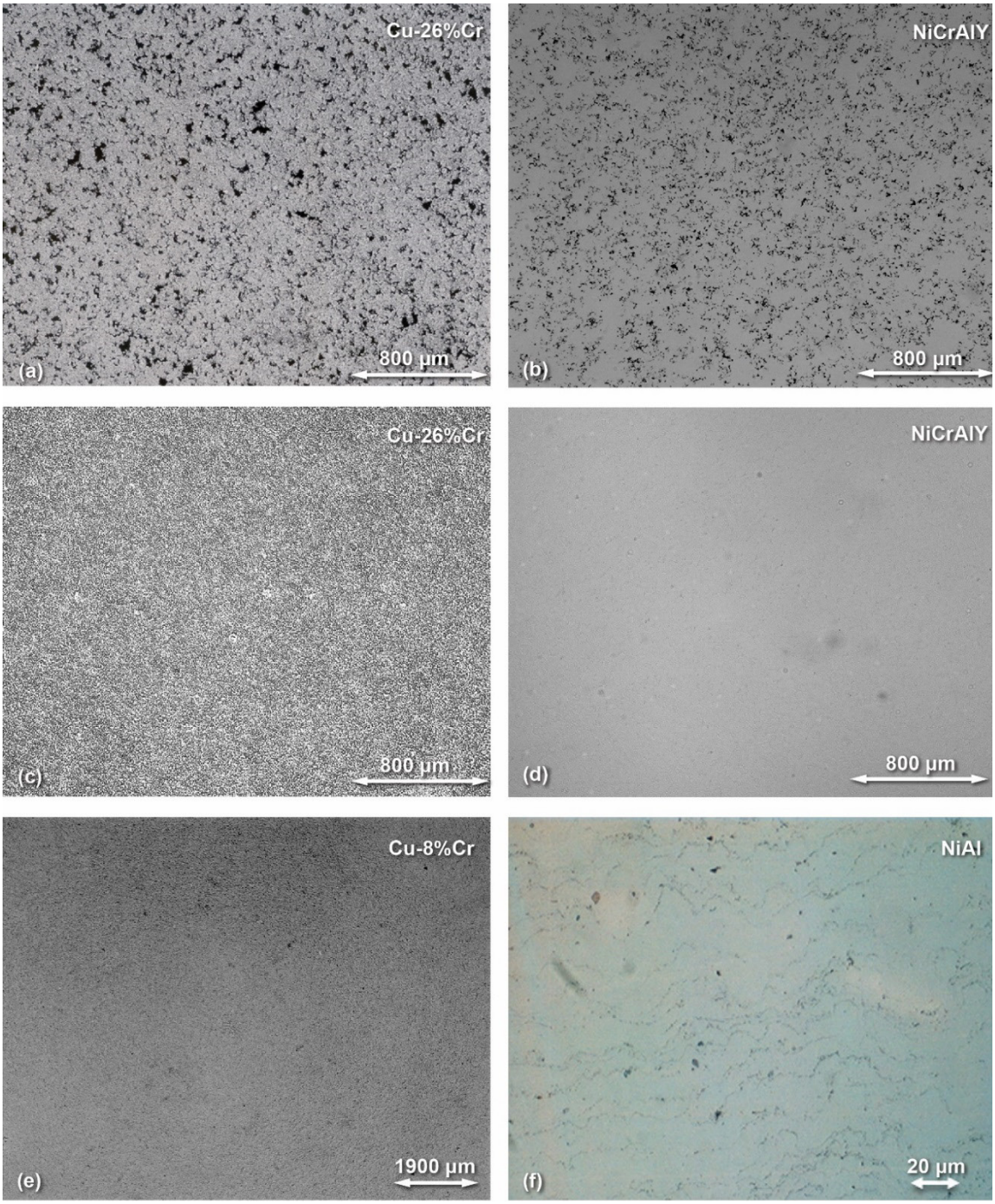

Figure 1.—Microstructures of vacuum plasma sprayed monolithic coatings: (a) Cu-26%Cr (V2-02-27A); (b) Ni-17%Cr-6%Al-0.5%Y (V2-02-27E); (c) Cu-26%Cr (V2-03-524); (d) Ni-17%Cr-6%Al-0.5%Y (V2-03-528); (e) Cu-8%Cr (V2-03-134); and (f) stoichiometric NiAl (V2-03-143).

TABLE II.—MAGNITUDES OF ROOM TEMPERATURE BULK DENSITY OF DIFFERENT SPRAYED MONOLITHIC COATINGS

Nominal coating composition[a]	Batch I.D.	Processed condition	Bulk density,[b] kg/m^3
Cu-8(at.%)Cr-4%Nb	GRCop-84	Extruded	8945
Cu-8(wt.%)Cr	V2-03-134	VPS	8598
Cu-26(wt.%)Cr[3]	V2-02-27B	VPS	5450
Cu-26(wt.%)Cr	V2-03-524	VPS	5826
Cu-8(wt.%)Cr-1%Al	V2-05-27	VPS	8546
Cu-17(wt.%)Cr-5%Al	8	As-cast	7688
Cu-23(wt.%)Cr-5%Al	Cu-23Cr-5Al	CS	7575
Ni-50(at.%)Al	V2-03-166	VPS	5826
Ni-17(wt.%)Cr-6%Al-0.5%Y[c]	V2-02-27E	VPS	7161
Ni-17(wt.%)Cr-6%Al-0.5%Y	V2-03-528	VPS	7711

[a]All compositions are in weight percent (wt.%) except those for GRCop-84 and NiAl for which the compositions are reported in atomic percent (at.%) as per convention.
[b]Calculated from the ratio of the mass to the geometric volume of the specimen.
[c]These specimens had a lot of porosity. All other sprayed specimens were close to 100% density.

whereas the α-Cu matrix in extruded GRCop-84 is strengthened by fine Cr_2Nb precipitates. The volume fraction of the α-Cr precipitates is higher in VPS Cu-26%Cr compared to the VPS Cu-8%Cr alloy. The microstructure of the as-cast Cu-17%Cr-5%Al alloy was reported elsewhere (Ref. 20), where the α-(Cu,Al) matrix contained a dispersion of α-Cr dendrites.

3.2 Thermal Diffusivity

Figure 2 compares the temperature dependence of α for extruded GRCop-84, VPS Cu-8%Cr, VPS Cu-26%Cr, VPS Cu-8%Cr-1%Al, as-cast Cu-17%Cr-5%Al and CS Cu-23%Cr-5%Al. The magnitudes of α vary between 5×10^{-5} and 1×10^{-4} m^2/s at 300 K for these materials. A close examination of the data reveals that the thermal diffusivity data for the VPS Cu-8%Cr, VPS Cu-26%Cr and hot-extruded GRCop-84 specimens show a gradual decrease with increasing temperature whereas the curve for the VPS Cu-8%Cr-1%Al coating initially increases gradually with increasing temperature until about 800 K before decreasing with continued increase in temperature to thermal diffusivity values close to those of Cu-8%Cr, Cu-26%Cr and GRCop-84. The two sets of data for the VPS Cu-26%Cr monolithic coatings differ from each other significantly since batch V2-02-27B is significantly more porous (Figure 1(a) than batch V2-03-524 (Figure 1(c)), and therefore, it has a lower thermal diffusivity. The thermal diffusivity of the as-cast Cu-17%Cr-5%Al alloy increases slightly with increasing absolute temperature from $\alpha\sim2.0\times10^{-5}$ m^2/s at 296 K to $\alpha\sim2.9\times10^{-5}$ m^2/s at 1223 K with the magnitudes of α are significantly lower than those for the other copper alloys. As expected, the magnitudes of α for the CS Cu-23%Cr-5%Al coating are similar during the heat-up and cool-down portion of the cycle within the limits of experimental scatter. The data were regression fitted empirically using the polynomial Equation (4)

$$\alpha = A_\alpha * T^4 + B_\alpha * T^3 + C_\alpha * T^2 + D_\alpha * T + E_\alpha \tag{4}$$

where A_α, B_α, C_α, D_α, and E_α are regression coefficients, and R_d^2 are coefficients of determination (Table III).

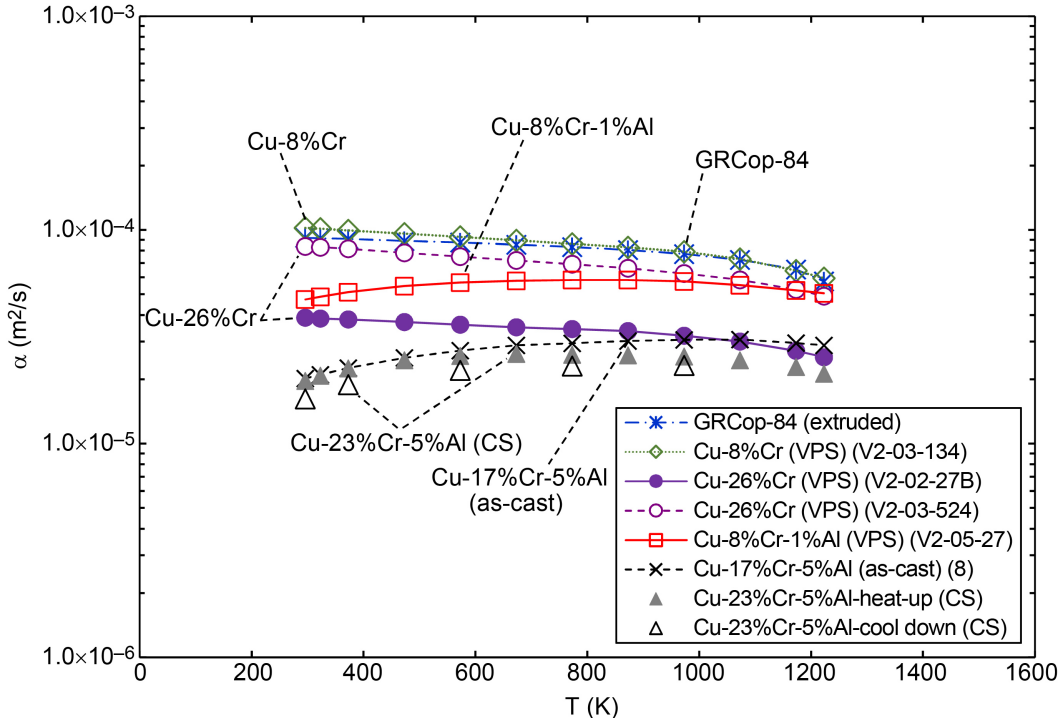

Figure 2.—Temperature dependences of the thermal diffusivities of extruded GRCop-84, VPS Cu-8%Cr, VPS Cu-26%Cr (V2-02-27B and V2-03-524), VPS Cu-8%Cr-1%Al, as-cast Cu-17%Cr-5%Al (8), and CS Cu-23%Cr-5%Al during the heat-up and cool down cycle.

TABLE III.—REGRESSION COEFFICIENTS FOR THE TEMPERATURE DEPENDENCE OF THERMAL DIFFUSIVITY DESCRIBED BY EQUATION (4)

Material	A_α, $m^2/K^4 \cdot s$	B_α, $m^2/K^3 \cdot s$	C_α, $m^2/K^2 \cdot s$	D_α, $m^2/K \cdot s$	E_α, m^2/s	R_d^2
GRCop-84 (extruded) ($296 \le T \le 1223$ K)	-1.5×10^{-16}	3.8×10^{-13}	-3.6×10^{-10}	1.3×10^{-7}	7.7×10^{-5}	0.9977
Cu-8%Cr (V2-03-134) ($296 \le T \le 1223$ K)	-9.5×10^{-17}	2.2×10^{-13}	-1.8×10^{-10}	3.0×10^{-8}	1.0×10^{-4}	0.9999
Cu-26%Cr (V2-02-27B) ($296 \le T \le 1223$ K)	-2.6×10^{-17}	5.1×10^{-14}	-3.3×10^{-11}	-1.7×10^{-9}	4.1×10^{-5}	0.9993
Cu-26%Cr (V2-03-524) ($296 \le T \le 1223$ K)	-5.6×10^{-17}	1.3×10^{-13}	-1.1×10^{-10}	7.5×10^{-9}	8.8×10^{-5}	0.9999
Cu-8%Cr-1%Al (V2-05-27) ($296 \le T \le 1223$ K)	-4.8×10^{-17}	1.5×10^{-13}	-2.2×10^{-10}	1.5×10^{-7}	1.8×10^{-5}	0.9989
Cu-17%Cr-5%Al (as-cast) (8) ($296 \le T \le 1223$ K)	-3.4×10^{-17}	1.0×10^{-13}	-1.4×10^{-10}	9.5×10^{-8}	1.3×10^{-6}	0.9989
Cu-23%Cr-5%Al-(CS) (heat-up) ($296 \le T \le 1223$ K)	-7.3×10^{-17}	2.3×10^{-13}	-2.9×10^{-10}	1.6×10^{-7}	-8.6×10^{-6}	0.9987
NiAl (V2-03-166) ($296 \le T \le 1223$ K)	3.2×10^{-18}	-1.2×10^{-14}	1.2×10^{-11}	-1.1×10^{-9}	1.8×10^{-5}	0.9889
Ni-17%Cr-6%Al-0.5%Y (V2-02-27E) ($296 \le T \le 1223$ K)	-4.5×10^{-18}	6.7×10^{-15}	-1.4×10^{-12}	1.6×10^{-9}	2.4×10^{-6}	0.9975
Ni-17%Cr-6%Al-0.5%Y (V2-03-528) ($296 \le T \le 1223$ K)	-5.1×10^{-18}	1.1×10^{-14}	-7.8×10^{-12}	5.3×10^{-9}	1.9×10^{-6}	0.9993

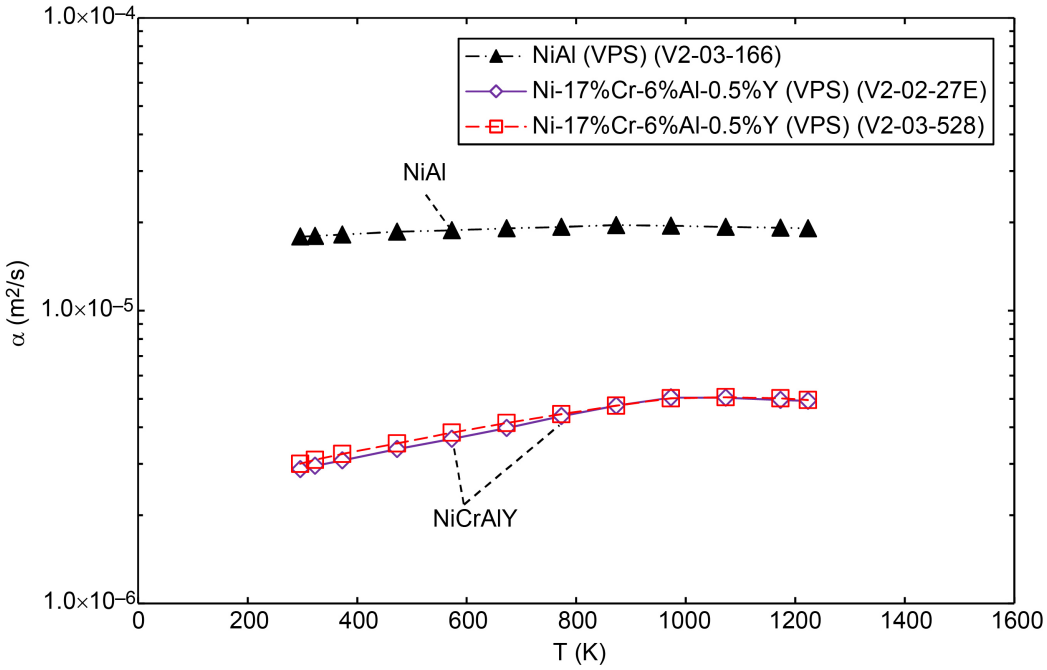

Figure 3.—Temperature dependences of the thermal diffusivities of stoichiometric VPS NiAl, and two VPS Ni-17%Cr-6%Al-0.5%Y (V2-02-27E and V2-03-528).

The thermal diffusivity of VPS NiAl is almost independent of temperature with the magnitudes of $\alpha \sim 1.8\times10^{-5}$ to 1.9×10^{-5} m^2/s between 296 and 1223 K (Figure 3). In contrast, the thermal diffusivity of the VPS NiCrAlY coating increases with increasing temperature from about 2×10^{-6} m^2/s at 296 K to 5×10^{-6} m^2/s at 1223 K. Interestingly, despite the differences in the porosity content, the magnitudes of α for the two batches of VPS NiCrAlY are nearly identical. Table III shows the magnitudes of the regression coefficients and R_d^2 for the monolithic VPS NiAl and the two batches of VPS NiCrAlY coatings.

3.3 Thermal Conductivity

Figure 4 shows the variation of K_T as a function of absolute temperature for extruded GRCop-84, VPS Cu-8%Cr, two batches of VPS Cu-26%Cr, VPS Cu-8%Cr-1%Al, as-cast Cu-17%Cr-5%Al, and CS Cu-23%Cr-5%Al. In addition, the temperature dependences of λ for VPS Cu-8%Cr-1%Al and CS Cu-23%Cr-5%Al are also shown in the figure. The magnitudes of K_T are represented by the left hand axis while the data for λ are represented by the right hand axis as denoted by the arrows. It is important to note that despite the fact that K_T and λ were determined by two different techniques, the two sets of data match very nicely for both VPS Cu-8%Cr-1%Al and CS Cu-23%Cr-5%Al.

The values of K_T decrease with increasing T for the VPS Cu-8%Cr and for the low porosity VPS Cu-26%Cr coatings (V2-03-524), whereas K_T increases slightly up to 673 K for extruded GRCop-84 before decreasing with increasing T when T > 673 K. The magnitudes of K_T vary between about 345 W/m/K at 296 K and about 245 W/m/K at 1223 K for the VPS Cu-8%Cr coating. The values of K_T for the VPS Cu-26%Cr coating (V2-03-524) are significantly lower varying between about 285 W/m/K at 296 K and 210 W/m/K at 1223 K. As expected, the presence of porosity in the VPS Cu-26%Cr batch V2-02-27B significantly decreases the thermal conductivity of VPS Cu-26%Cr by factors of 3.4 and 2.9 at 296 and 1223 K, respectively, compared to batch V2-03-524. In this case, the magnitude of K_T decreases from about 85 W/m/K at 296 K to about 72 W/m/K at 1223 K. The value of K_T for the extruded GRCop-84 at

296 K is about 315 W/m/K but increases to values similar to those for the VPS Cu-8%Cr coating above 673 K. In the case of Cu-8%Cr-1%Al, λ increases from about 100 W/m/K at about 92 K to about 179 W/m/K at 395 K while K_T increases from about 165 W/m/K at 296 K to about 235 W/m/K at 1223 K. The magnitudes of K_T for the as-cast Cu-17%Cr-5%Al increases from about 64 W/m/K at 296 K to about 116 W/m/K at 1223 K. These values are close to the magnitudes of K_T for the CS Cu-23%Cr-5%Al coating for which K_T vary between about 65 W/m/K at 296 K to about 97 W/m/K at 1223 K. As shown in Figure 4, the magnitudes of λ for the CS Cu-23%Cr-5%Al vary from about 32 W/m/K at about 90 K to about 80 W/m/K at about 459 K, and these data are in very good agreement with the values of K_T.

The K_T and λ data for the copper alloys shown in Figure 4 were regression fitted using the polynomial Equation (5)

$$K_T \text{ or } \lambda = A_i * T^4 + B_i * T^3 + C_i * T^2 + D_i * T + E_i \quad (5)$$

where A_i, B_i, C_i, D_i, and E_i are regression coefficients, the subscript i is either K or λ for high and low temperature conductivity, respectively.[3] Table IV gives the values of the regression coefficients, the corresponding magnitudes of R_d^2 and the temperature ranges for which the regression parameters is valid.

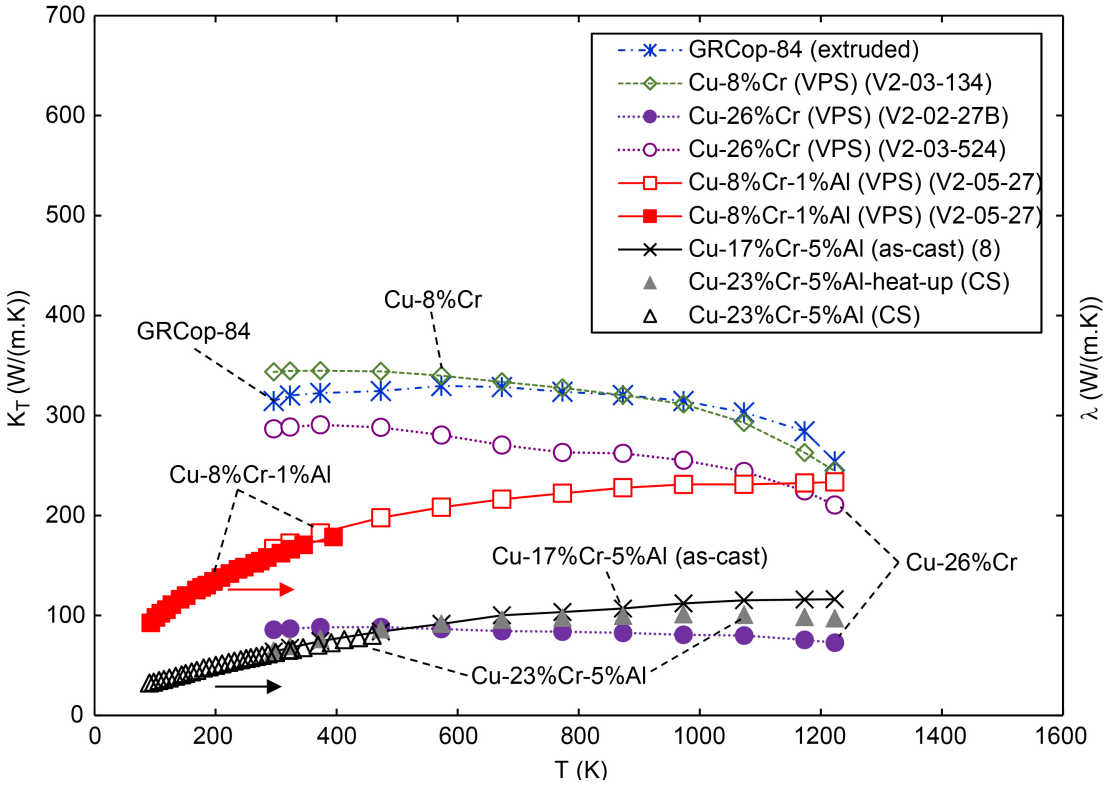

Figure 4.—Temperature dependences of the low (λ) and high thermal conductivities (K_T) for as-extruded GRCop-84, and VPS Cu-8%Cr, VPS Cu-26%Cr (V2-03-524), VPS Cu-8%Cr-1%Al, Cu-17%Cr-5%Al (as-cast) and CS Cu-23%Cr-5%Al. The low temperature thermal conductivity data for VPS Cu-8%Cr-1%Al and CS Cu-23%Cr-5%Al are denoted by the horizontal arrows.

[3] Although the individual values of K_T are derived from the values of α and C_P at each temperature, it is important to note that the purposes of the empirical regression equations such as Equation (5) are solely to identify the lowest order polynomial equations that accurately represent the data shown in Figure 2 to Figure 5 despite an inconsistency in the algebraic exponents.

TABLE IV.—REGRESSION COEFFICIENTS FOR THE TEMPERATURE DEPENDENCE OF TEMPERATURE THERMAL CONDUCTIVITY DESCRIBED BY EQUATION (5)

The subscripts K and λ are for high and low temperature thermal conductivity, respectively

Material	A_K or A_λ, W/m•K^5	B_K or B_λ, W/m•K^4	C_K or C_λ, W/m•K^3	D_K or D_λ, W/m•K^2	E_K or E_λ, W/m•K	R_d^2
GRCop-84 (extruded) ($296 \le T \le 1223$ K)	-7.4×10^{-10}	2.0×10^{-6}	-2.1×10^{-3}	9.6×10^{-1}	170.0	0.9808
Cu-8%Cr (V2-03-134) ($296 \le T \le 1223$ K)	-5.2×10^{-10}	1.4×10^{-6}	-1.4×10^{-3}	5.6×10^{-1}	266	0.9996
Cu-26%Cr (V2-02-27B) ($296 \le T \le 1223$ K)	-2.1×10^{-10}	6.4×10^{-7}	-7.1×10^{-4}	3.2×10^{-1}	388	0.9951
Cu-26%Cr (V2-03-524) ($296 \le T \le 1223$ K)	-8.2×10^{-10}	2.4×10^{-6}	-2.5×10^{-3}	1.0	140	0.9982
Cu-8%Cr-1%Al (V2-05-27) ($296 \le T \le 1223$ K)	-7.7×10^{-11}	3.2×10^{-7}	-5.4×10^{-4}	4.7×10^{-1}	693	0.9994
Cu-8%Cr-1%Al (V2-05-27) ($92 \le T \le 395$ K)	-1.1×10^{-8}	1.2×10^{-5}	-5.0×10^{-3}	1.2	137	0.9998
Cu-17%Cr-5%Al (as-cast) (#8) ($296 \le T \le 1223$ K)	-9.9×10^{-11}	3.4×10^{-7}	-4.6×10^{-4}	3.4×10^{-1}	–5.21	0.9987
Cu-23%Cr-5%Al (CS) ($296 \le T \le 1223$ K)	-2.1×10^{-10}	6.9×10^{-7}	-8.9×10^{-4}	5.4×10^{-1}	–34.3	0.9996
Cu-23%Cr-5%Al (CS) ($90 \le T \le 459$ K)	1.4×10^{-9}	-1.3×10^{-6}	2.8×10^{-4}	1.5×10^{-1}	17.0	0.9997
NiAl (V2-03-166) ($296 \le T \le 1223$ K)	1.0×10^{-11}	-3.8×10^{-8}	2.6×10^{-5}	2.6×10^{-2}	48.3	0.9984
NiAl (V2-03-166) ($82 \le T \le 399$ K)	-4.3×10^{-9}	4.8×10^{-6}	-2.0×10^{-3}	4.2×10^{-1}	8.99	0.9989
Ni-17%Cr-6%Al-0.5%Y (V2-02-27E) ($296 \le T \le 1223$ K)	-6.3×10^{-11}	1.6×10^{-7}	-1.5×10^{-4}	6.7×10^{-2}	–1.24	0.9983
Ni-17%Cr-6%Al-0.5%Y (V2-03-528) ($296 \le T \le 1223$ K)	-6.3×10^{-11}	2.0×10^{-7}	-2.0×10^{-4}	1.0×10^{-1}	–6.69	0.9998

The approximate similarity in the magnitudes of K_T for VPS Cu-8%Cr and extruded GRCop-84 observed in Figure 4 suggests that the differences in the processing conditions, precipitate composition (i.e., Cr_2Nb in GRCop-84 and α-Cr in Cu-8%Cr) and precipitate size and morphology do not significantly affect the high temperature thermal conductivity of these alloys. Increasing the Cr content from 8 to 26% decreases the high temperature conductivity of the Cu-Cr alloys to some extent, but the presence of large amounts of porosity in the microstructure significantly decreases K_T by a large amount. Interestingly, the addition of 1%Al to the Cu-8%Cr alloy results both in a considerable decrease in thermal conductivity at the lower temperatures and in the nature of its temperature dependence. Increasing the Al content to 5% further decreases the thermal conductivity of the Cu-Cr alloys irrespective of processing conditions and Cr content. Since the magnitudes of K_T are approximately similar for the porous VPS Cu-26%Cr (V2-02-27B), as-cast Cu-17%Cr-5%Al and CS Cu-23%Cr-5%Al, it appears that both matrix voids and Al atoms in solid solution scatter the lattice phonons and electrons more significantly than the Cr_2Nb precipitates in the extruded GRCop-84 and the α-Cr precipitates in the VPS Cu-8%Cr and Cu-26%Cr.

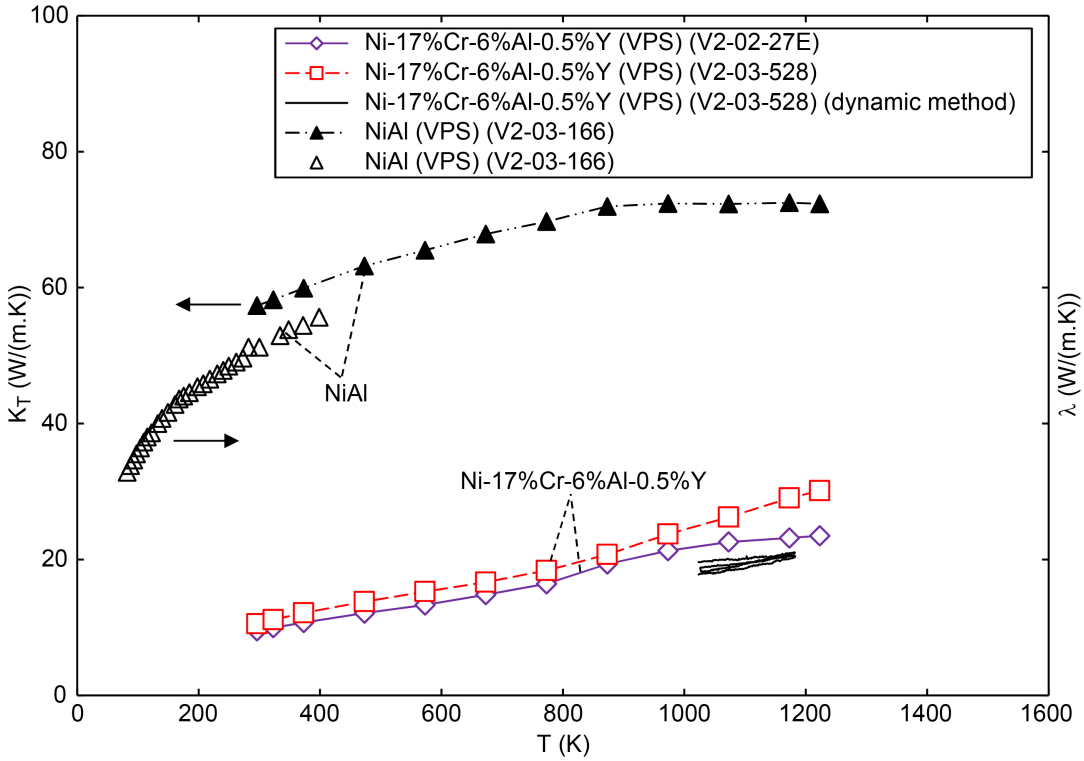

Figure 5.—Temperature dependences of the low (λ) and high thermal conductivities (K_T) for stoichiometric VPS NiAl, and two VPS Ni-17%Cr-6%Al-0.5%Y (V2-02-27E and V2-03-528) measured by the laser flash method. NiCrAlY (V2-03-528) (GRC) refers to data obtained by the dynamic measurement technique.

Figure 5 shows temperature dependences of K_T and λ for VPS NiAl and the two batches of VPS NiCrAlY determined by the laser flash technique. In addition, thermal conductivity data on VPS NiCrAlY (V2-03-528) from the dynamic laser measurement method are also shown in the figure. Comparison of Figure 4 and Figure 5 reveals that these Ni-based coatings exhibit much lower thermal conductivities than the copper alloys. The values of λ for NiAl increase from about 33 W/m/K at 82 K to about 56 W/m/K at 399 K while K_T increases from about 57 W/m/K at 296 K to about 72 W/m/K at 1223 K. At 300 K, λ ~ 51 W/m/K for NiAl and this value is slightly lower the room temperature magnitude of K_T. In the case of NiCrAlY (V2-03-528), the magnitude of K_T increases from about 11 W/m/K at 296 K to about 30 W/m/K at 1223K. The second NiCrAlY batch (V2-02-27E), which had considerably more porosity (Figure 1(b)), exhibits similar values of K_T between 296 and 1073 K but attains an approximately constant value of K_T ~ 24 W/m/K at and above 1073 K. Interestingly, the magnitudes of K_T determined by the dynamic method are lower than those determined by the laser flash method for NiCrAlY (V2-03-528). The precise reason for this difference in the two sets of data is unclear. Clearly, unlike in the case of Cu-26%Cr (Figure 4), the presence of voids in the NiCrAlY did not significantly affect the magnitudes of the measured K_T below 973 K presumably because NiCrAlY has much lower thermal conductivity than Cu-26%Cr. Above 973 K, the effect of porosity became more significant as the curve for NiCrAlY batch V2-02-27E tends towards a constant value of K_T independent of temperature. Table IV shows the values of regression coefficients and R_d^2 for the nonlinear regression fits to the data shown in Figure 5 using Equation (5).

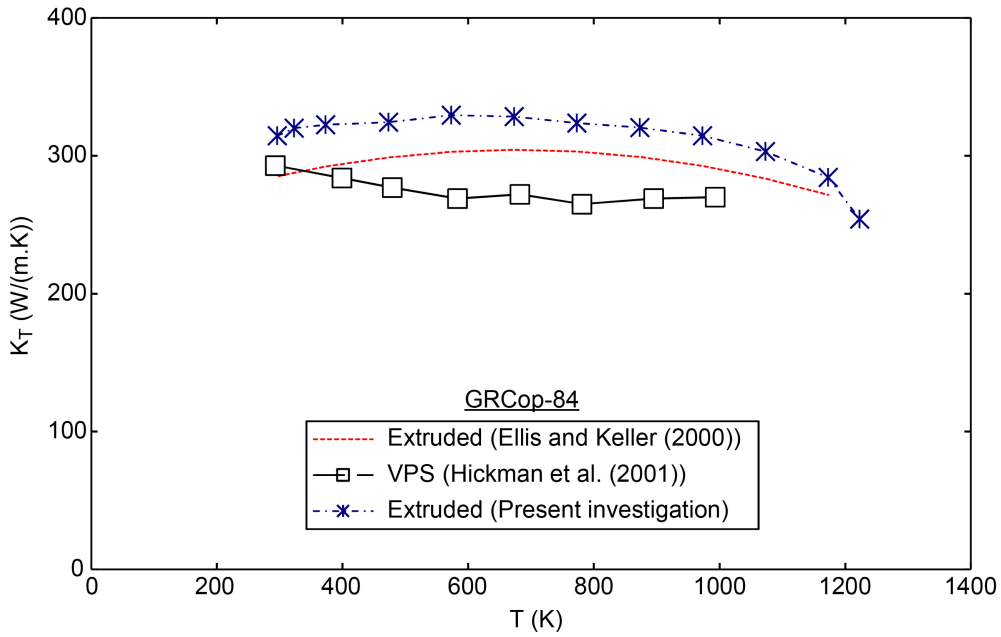

Figure 6.—Comparison of the temperature dependence of the high temperature thermal conductivity of extruded GRCop-84 reported in the present investigation with those for extruded (Ref. 7) and VPS (Ref. 9) GRCop-84.

3.4 Comparison With High Temperature Thermal Conductivity Literature Data

Other than GRCop-84, there appears to be no prior literature data reported on the Cu alloys investigated in the present study. Figure 6 compares the present data on K_T with those reported for extruded (Ref. 7) and VPS (Ref. 9) GRCop-84. Since there was significant batch-to-batch scatter in the reported values of K_T for extruded GRCop-84, the line in Figure 6 represents the weighted regression equation for all the data published by Ellis and Keller (Ref. 7). The VPS data represent those reported for the –325 mesh powder lot (Ref. 9). The present data are in reasonable agreement with the literature data within the large scatter band reported in the literature (Ref. 7).

Figure 7 compares the temperature dependence of K_T reported in the present investigation for VPS NiAl with those reported for single crystal NiAl (Ref. 41). Above 773 K, the two sets are in agreement within about 10%. The present observations are significantly lower than those reported for single crystal NiAl below 773 K, where the two sets of data increasingly deviate from each other with decreasing temperature, presumably due to scattering at extrinsic defects such as grain and splat boundaries, impurities and voids in the thermally sprayed coating.

Figure 8 compares the three sets of data reported in the present paper with those reported by Holmes and McKechnie (Refs. 24 and 25) on VPS Ni-17%Cr-6%Al-0.5%Y. An examination of Figure 8 reveals that the values of K_T determined in the present investigation are comparable to those reported by Holmes and McKechnie (Refs. 24 and 25) below 573 K but the deviation between the present data and those reported by Holmes and McKechnie (Refs. 24 and 25) increases with increasing temperature, where the values reported in this paper are significantly higher. One plausible reason for the observed differences in K_T is that there were large differences in the density of pores. The measured density of the VPS NiCrAlY investigated by Holmes and McKechnie (Refs. 24 and 25) was about 5500 kg/m^3, which is much lower than the values shown in Table II by 30 to 40% thereby indicating a significantly more porous coating than those studied in the present investigation. This observation is consistent with the fact that batch V2-02-27E, which was more porous (Figure 1(b)) than batch V2-03-528 (Figure 1(d)), exhibits lower values

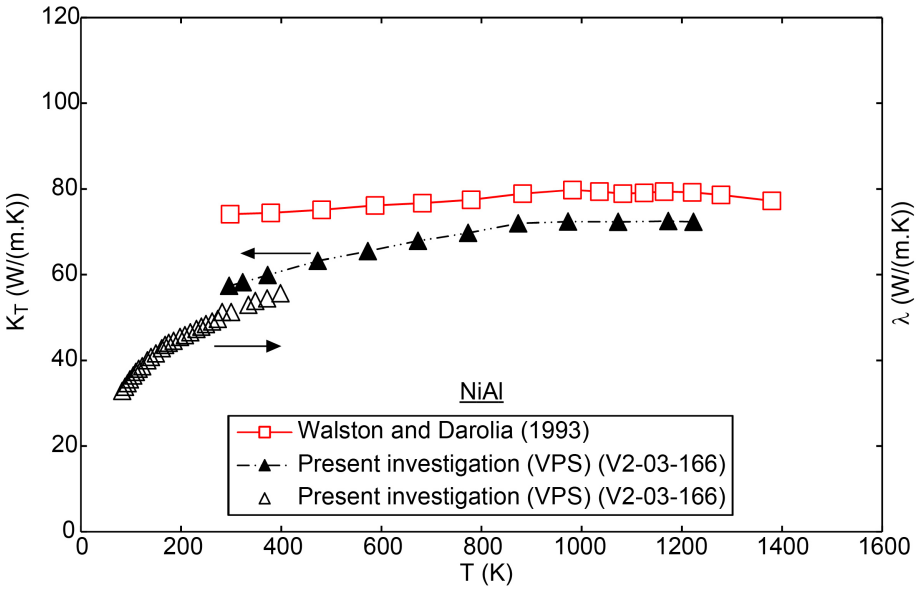

Figure 7.—Comparison of the temperature dependence of the high temperature thermal conductivity of VPS NiAl reported in the present investigation with those for single crystal NiAl (Ref. 42).

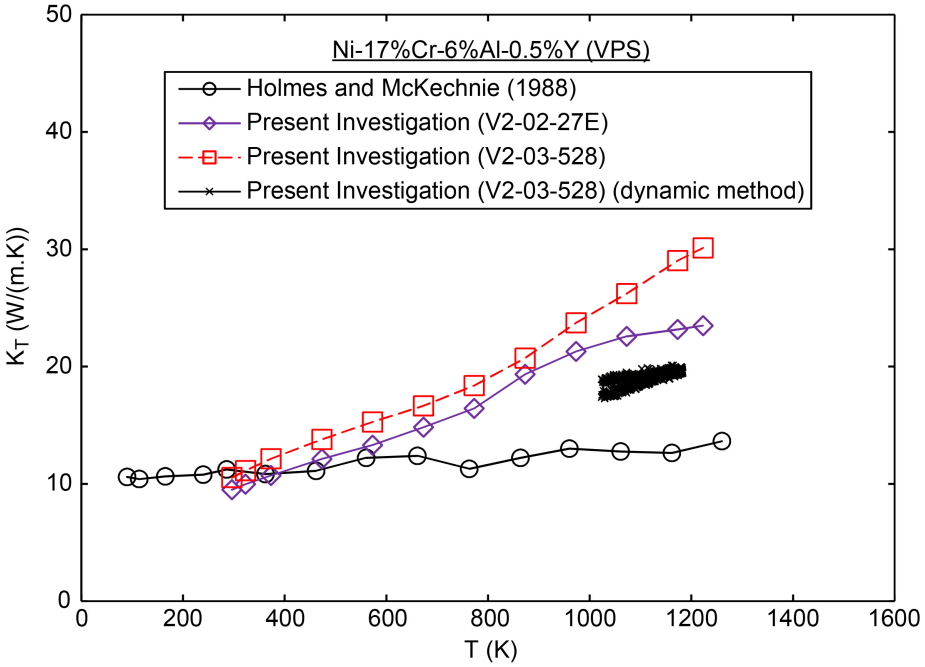

Figure 8.—Comparison of the temperature dependence of the high temperature thermal conductivity of VPS Ni-17%Cr-6%Al-0.5%Y reported in the present investigation and in the literature (Refs. 25 and 26).

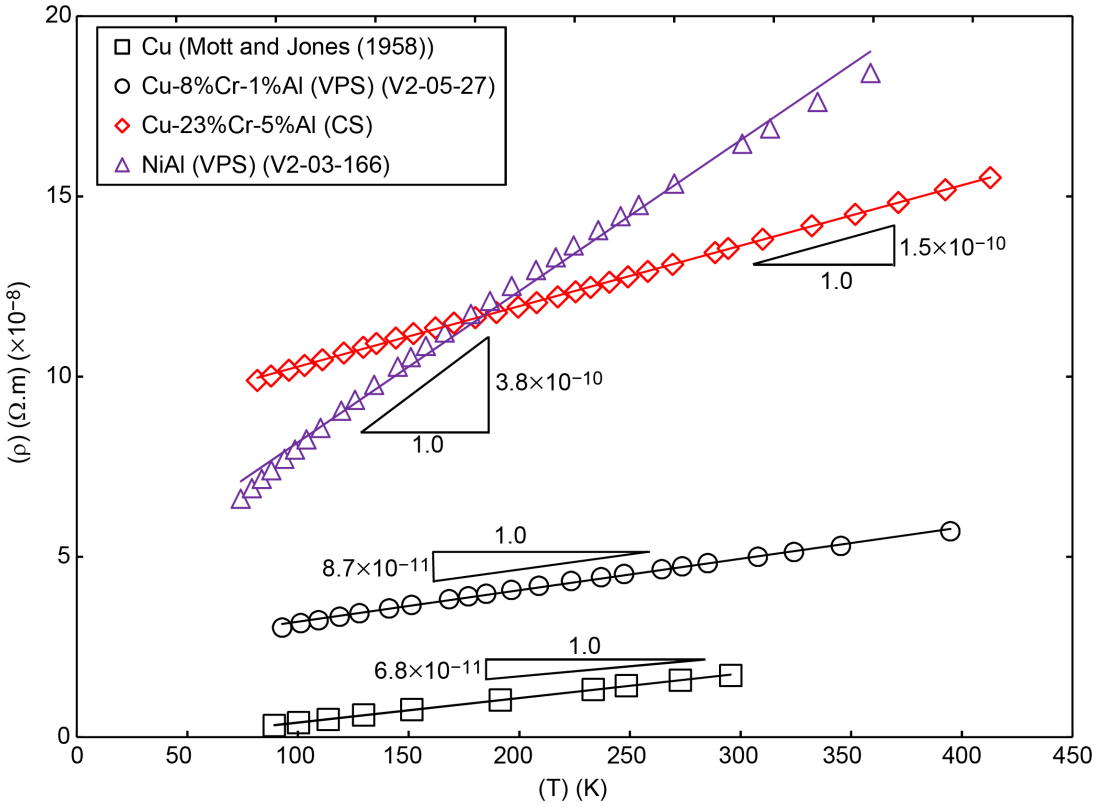

Figure 9.—Temperature dependencies of the electrical resistivity for VPS Cu-8%Cr-1%Al, CS Cu-23%Cr-5%Al and VPS NiAl. The solid lines through the data represent linear regression fits to the data. Literature data on Cu is also shown (Ref. 43).

of K_T above 973 K. The close agreement in the magnitudes of K_T below 573 K for all the coatings, and below 973 K for the two batches studied in the present investigation, suggests that the dominant thermal conductivity mechanism is sensitive to the density of voids only at high temperatures. Since thermal conductivity in metallic alloys are mainly determined by electron mobility (Refs. 42, 44, 46 to 50), it is reasonable to conclude that the observed lower values of K_T observed in more porous batches of the Cu-26%Cr and NiCrAlY coatings are due to electron-porosity scattering.

3.5 Temperature Variation of Electrical Resistivity

Figure 9 shows the variation of the electrical resistivity with absolute temperature for VPS Cu-8%Cr-1%Al, CS Cu-23%Cr-5%Al and VPS NiAl between about 100 and 500 K with the linear regression fit represented by the solid lines. The slopes of these regression lines are depicted in the figure. The figure also shows literature data on Cu for comparison (Ref. 51). The electrical resistivities of these three coatings are higher than those of Cu. The resistivity of the Cu-8%Cr-1%Al coating, which is significantly lower than that of Cu-23%Cr-5%Al and NiAl, varied between 3.0×10^{-8} Ω.m at 92.9 K and 5.7×10^{-8} Ω.m at 394.9 K. In comparison, the electrical resistivity, $\rho_{Cu23Cr5Al}$, of the Cu-23%Cr-5%Al coating varied between 9.9×10^{-8} Ω.m at 90.7 K and 1.6×10^{-7} Ω.m at 458.7 K. Similarly, the values of electrical resistivity, ρ_{NiAl}, for the NiAl coating varied between 6.6×10^{-8} Ω.m at 82.4 K and 1.8×10^{-7} Ω.m at 398.6 K. Since the electrical resistivity of NiAl exhibits a stronger temperature variation than Cu-23%Cr-5%Al, the two plots cross each other at about 200 K so that $\rho_{NiAl} < \rho_{Cu23Cr5Al}$ when $T < 200$ K.

Matthiessen's rule states that the electrical resistivity can be expressed as (Refs. 42, 44, 46 to 50)

$$\rho = \rho(T) + \rho_c \tag{6}$$

where $\rho(T)$ is temperature dependent component of electrical resistivity due to electron-phonon scattering and ρ_c is the temperature independent residual electrical resistivity due to electron-impurity scattering by impurities of a dilute concentration, c. Since Matthiessen's rule is not always observed, an additional term is often added to Equation (6) (Refs. 42, 44, and 48)

$$\rho = \rho(T) + \rho_c + \Delta\rho(c,T) \tag{7}$$

where $\Delta\rho(c,T)$ accounts for the deviation between the experimental data and Equation (6). Above the Debye temperature, θ_D, for a nonmagnetic metal or alloy, the temperature dependence of $\rho(T)$, which is due to electron-phonon scattering, is generally expressed as (Refs. 28, 31, 42, 44, 47, 48, and 52)

$$\rho(T) = \rho_0 (1 + \beta(T - T_0)) \tag{8}$$

where T is the absolute temperature, T_0 is the reference temperature, ρ_0 is the resistivity at T_0, and β is the temperature coefficient of the resistivity. The linear temperature dependence given by Equation (8) is not always followed, and in this case, empirical polynomial fits are used (Refs. 47, 52, and 53). It is noted that other electron scattering mechanisms are important at $T < \theta_D$, where $\rho(T) \propto T^n$ with n = 2, 3 or 5 depending on the characteristics of the electron scattering mechanism predicted by the Bloch-Grüneisen equation (Refs. 46, 48, and 54).

Figure 10 shows the variation of $(\rho - \rho_0)$ with $(T - T_0)$ for VPS Cu-8%Cr-1%Al, CS Cu-23%Cr-5%Al and VPS NiAl, where the experimental values of ρ_0 and T_0 for each alloy are given in Table V.[4] The values of β shown in Table V were determined by fitting Equation (8) to the experimental data. The corresponding values of R_d^2 are also shown in Table V. A close examination of Figure 10 reveals that the linear temperature dependence of $(\rho - \rho_0)$ predicted by Equation (8) is closely matched by the data for the two copper alloys whereas the data for NiAl significantly deviates from the linear regression line represented by Equation (8). Since non-linear temperature dependencies of $\rho(T)$ are predicted by the Bloch-Grüneisen theory (Refs. 46, 48, and 54), Equation (9) was used to fit the data shown in Figure 10.

$$\rho(T) = \rho_0 (1 + \beta_1 (T - T_0) + \beta_2 (T - T_0)^2 + \beta_3 (T - T_0)^3) \tag{9}$$

where β_1, β_2 and β_3 are temperature coefficients of resistivity. Table VI gives the values of β_1, β_2, β_3 and R_d^2. It is clear through a comparison of the values of R_d^2 in Table V and Table VI, Equation (9) fits the data in Figure 10 much better than Equation (8) especially for NiAl. These observations suggest that other electron scattering processes (e.g., electron-electron scattering) may have contributed to the experimental measurements in addition to the high temperature electron-phonon scattering mechanism.

[4] A plot of $(\rho - \rho_0)$ against $(T - T_0)$ essentially cancels the contribution of ρ_c to ρ.

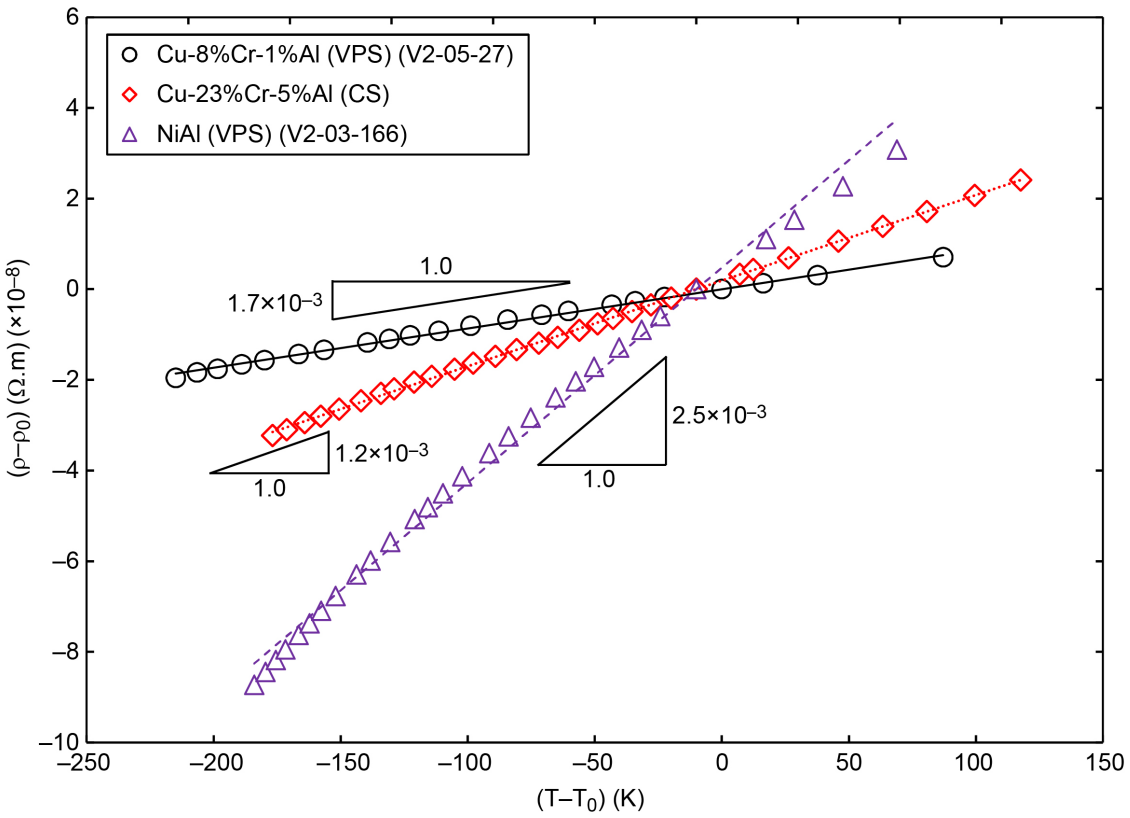

Figure 10.—Variation of $(\rho - \rho_0)$ with $(T - T_0)$ for VPS Cu-8%Cr-1%Al, CS Cu-23%Cr-5%Al and VPS NiAl. The regression lines represent the fit of Equation (8) to the experimental data.

TABLE V.—VALUES OF β AND R_d^2 DETERMINED BY FITTING EQUATION (8) TO THE DATA SHOWN IN FIGURE 10

Material	T_0, K	ρ_0, Ω m	β, Ω m/K	R_d^2
Cu-8%Cr-1%Al	307.8	5.0×10^{-8}	1.73×10^{-3}	0.99864
Cu-23%Cr-5%Al	299.2	13.1×10^{-8}	1.15×10^{-3}	0.99973
NiAl	300.0	15.4×10^{-8}	2.47×10^{-3}	0.99728

TABLE VI.—VALUES OF β_1, β_2, β_3 AND R_d^2 DETERMINED BY FITTING EQUATION (9) TO THE DATA SHOWN IN FIGURE 10

Material	T_0, K	ρ_0, Ω m	β_1, Ω m/K	β_2, Ω m/K^2	β_3, Ω m/K^3	R_d^2
Cu-8%Cr-1%Al (VPS)	307.8	5.0×10^{-8}	1.6×10^{-3}	3.6×10^{-8}	5.0×10^{-9}	0.99997
Cu-23%Cr-5%Al (CS)	299.2	13.1×10^{-8}	1.1×10^{-3}	4.0×10^{-8}	9.0×10^{-10}	0.99978
NiAl (VPS)	300.0	15.4×10^{-8}	2.1×10^{-3}	-1.3×10^{-6}	4.2×10^{-9}	0.99999

3.6 Application of the Wiedemann-Franz Law

Typically, for $T >> \theta_D$, the Wiedemann-Franz law is followed by a large number of metallic materials, where the carriers for electrical and thermal conduction are valence electrons (Refs. 28, 31, 42, 47, 49, 50, and 51). The law states that

$$\frac{\lambda}{\sigma_e} = L_0 T \tag{10}$$

where σ_e (= 1/ρ) is the electrical conductivity and L_0 is the Lorenz number with a theoretically derived constant Sommerfeld value of 2.45×10^{-8} WΩ/K^2 (Refs. 42, 47, 49, and 51). However, for $T << \theta_D$, the Lorenz number is no longer a universal constant and less than 2.45×10^{-8} WΩ/K^2 (Ref. 47).

Equation (10) suggests that the ratio λ/σ_e increases linearly with T. Figure 11 confirms this linear relationship and Table VII lists the values of L_0 determined by fitting Equation (10) to the data. The experimental magnitudes of L_0 are 2.64×10^{-8} WΩ/K^2 for VPS NiAl, 2.70×10^{-8} for VPS Cu-8%Cr-1%Al, and 2.79×10^{-8} WΩ/K^2 for CS Cu-23%Cr-5%Al. These values are higher than the theoretical Sommerfeld value by about 8 to 14% but compare very well with values reported for metals (Refs. 42, 50, and 51). Equation (10) assumes that L_0 is not dependent on temperature. In reality, deviations from the form of Equation (10) have been reported and discussed in detail in the literature (Refs. 28, 29, 31, 42, 50, and 51).

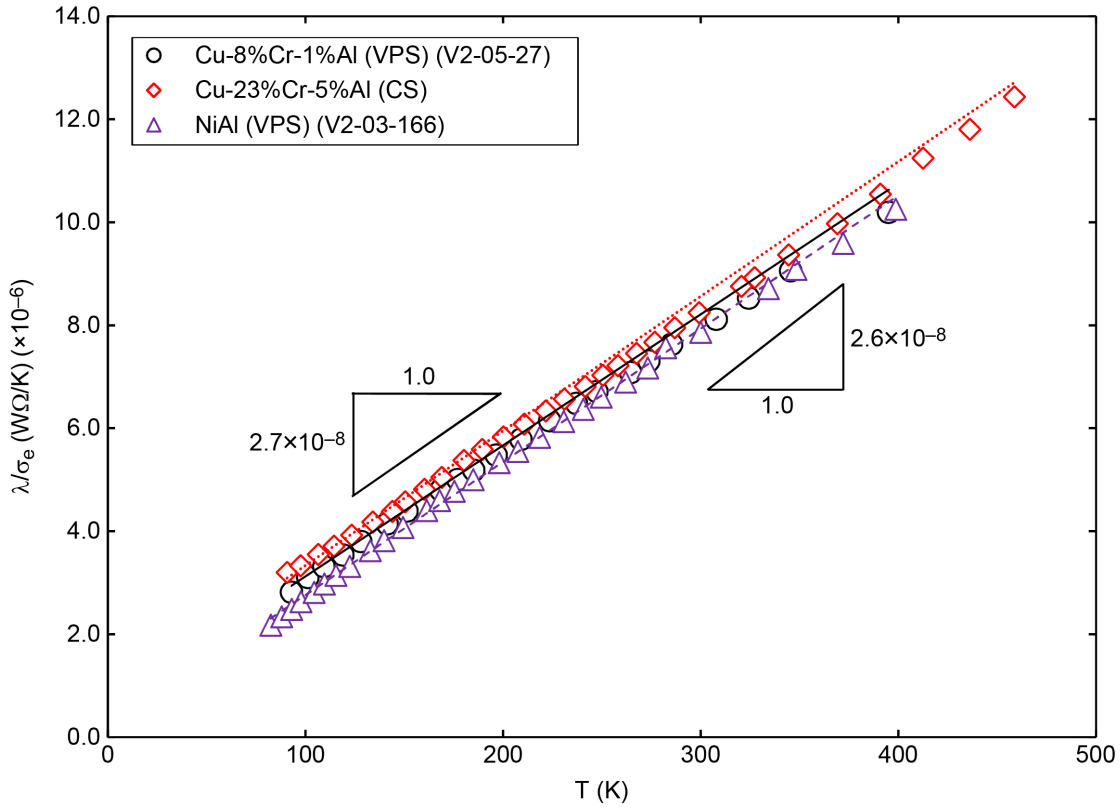

Figure 11.—Plot of the ratio of the low temperature thermal conductivity to electrical conductivity against absolute temperature for VPS Cu-8%Cr-1%Al, CS Cu-23%Cr-5%Al and VPS NiAl. The regression lines represent the fit of Equation (10) to the experimental data.

TABLE VII.—VALUES OF L_0 AND R_d^2 DETERMINED BY FITTING EQUATION (10) TO THE DATA IN FIGURE 11

Material	L_0, WΩ/K^2	R_d^2
Cu-8%Cr-1%Al (VPS)	2.70×10^{-8}	0.9841
Cu-23%Cr-5%Al (CS)	2.79×10^{-8}	0.9833
NiAl (VPS)	2.64×10^{-8}	0.9977

TABLE VIII.—VALUES OF L_0, B AND R_d^2 DETERMINED BY FITTING EQUATION (11) TO THE DATA IN FIGURE 11

Material	L_0, WΩ/K^2	B, WΩ/K	R_d^2
Cu-8%Cr-1%Al (VPS)	2.42×10^{-8}	6.88×10^{-7}	0.9996
Cu-23%Cr-5%Al (CS)	2.49×10^{-8}	8.28×10^{-7}	0.9994
NiAl (VPS)	2.56×10^{-8}	2.01×10^{-7}	0.9990

Smith and Palmer (Ref. 28) empirically analyzed their data using Equation (11)

$$\frac{\lambda}{\sigma_e} = L_0 T + B \tag{11}$$

where B is a constant. Later developments in the theory of heat conduction resulted in other forms of Equation (11) (Ref. 31):

$$\frac{\lambda}{\sigma_e} = L_0 T - C T^n \tag{12}$$

where C is a constant and $-1 \le n \le 0$ in Equation (12) (Ref. 31). The values of L_0 and B determined by fitting Equation (11) to the data shown in Figure 11 are tabulated in Table VIII. A comparison of Table VII and Table VIII reveals that the magnitudes of R_d^2 are higher thereby indicating that Equation (11) is a better fit to the data than Equation (10). Clearly, the constant B in Equation (11) is identified with $(-CT^n)$ in Equation (12). Since the experimental values of B shown in Table VIII are independent of absolute temperature, it suggests that $n \sim 0$ so that $C = -B$.

3.7 Temperature Dependence of the Total Hemispherical Emissivity

Figure 12 shows the temperature dependence of ε_H for vacuum plasma sprayed Cu-8(wt.%)Cr, Cu-26(wt.%)Cr, Cu-8(wt.%)Cr-1%Al and NiAl monolithic coatings. Also, shown are the effects of oxidation on the magnitudes of ε_H for the Cu-8(wt.%)Cr coating.[5] The data for heavily oxidized (Ref. 45) and electropolished (Ref. 43) Cu are also shown. The linear regression lines for each set of data are shown in the figure.[6] An examination of Figure 12 reveals that ε_H increases linearly with increasing T for the VPS

[5] The specimen was somewhat oxidized prior to measurement but the surface started brightening as it was heated under high vacuum. Thus, the emissivity measurements were made with the surface in three different conditions. The terms “heavily oxidized”, “lightly oxidized” and “bright” are used in a qualitative sense to indicate the relative conditions of the surface.

[6] The regression lines for NiAl are only for the open symbol data.

copper alloy coatings but it is essentially independent of temperature for VPS NiAl. This temperature dependence of ε_H is well-represented by

$$\varepsilon_H = mT + \varepsilon_0 \tag{13}$$

where m and ε_0 are regression coefficients listed in Table IX for each coating and surface condition. The Cu-8%Cr coating with a polished surface exhibits the lowest values of ε_H varying from 0.103 at 373 K to 0.220 at 920 K. After lightly oxidizing the surface, ε_H increases to 0.143 at 373 K and 0.309 at 920 K with a corresponding increase in the magnitude of m (Table IX). In comparison, a heavily oxidized surface results in significant increases in the magnitudes of ε_H and m (Table IX). In this case, ε_H increases from 0.257 at 373 K to 0.517 at 920 K. In comparison, the magnitudes of ε_H varied from 0.489 at 753 K to 0.621 at 1194 K for the Cu-26%Cr coating. Interestingly, the data for the heavily oxidized Cu-8%Cr coating and that for Cu-26%Cr are similar above 750 K presumably because the surface oxides are similar in composition. The values of ε_H for electropolished Cu increased from 0.009 at 179 K to 0.024 at 820 K (Ref. 43). The reported values of ε_H for heavily oxidized Cu varied from 0.49 at 592 K to 0.85 at 1035 K (Ref. 45).

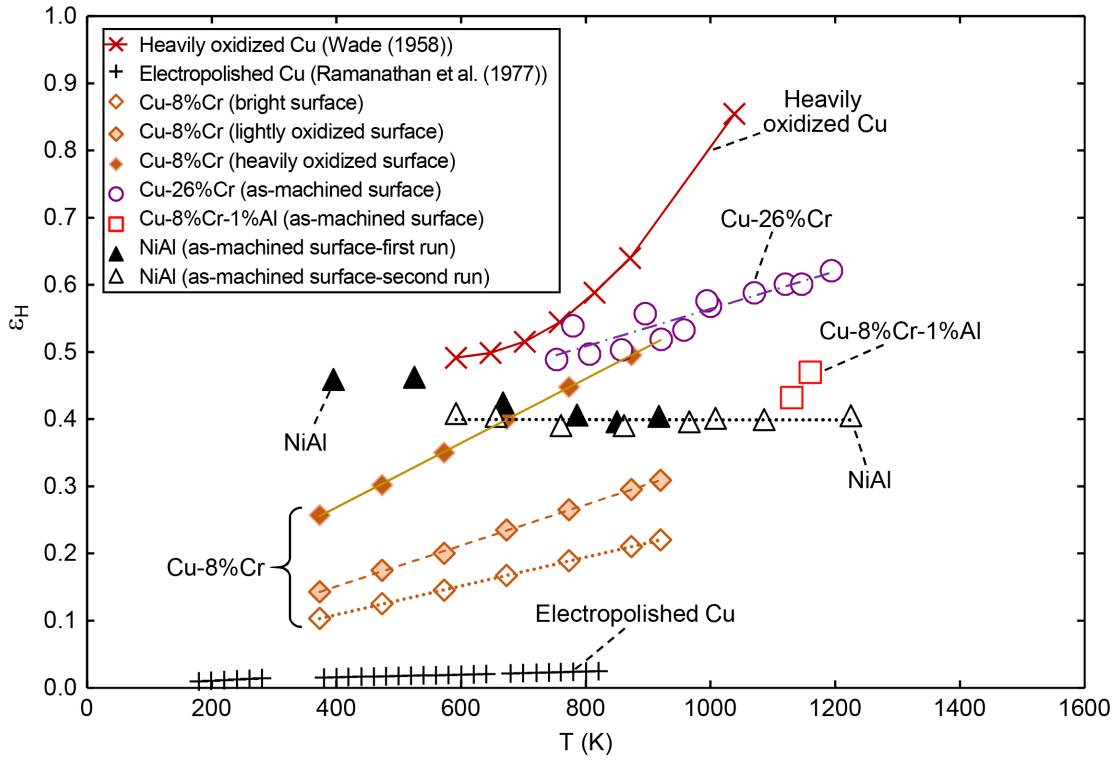

Figure 12.—Temperature dependence of total hemispherical emissivity for VPS Cu-8%Cr, VPS Cu-26%Cr (V2-03-524), VPS Cu-8%Cr-1%Al and VPS NiAl (V2-03-166). The effect of oxidation on ε_H is shown for the Cu-8%Cr coating.

TABLE IX.—VALUES OF m AND ε_0 FOR VPS MONOLITHIC COPPER ALLOY AND NiAl COATINGS

Material	Surface finish	m	ε_0	R_d^2
Cu-8%Cr	Polished	0.0002	0.0232	0.9999
Cu-8%Cr	Lightly oxidized	0.0003	0.0294	0.9992
Cu-8%Cr	Heavily oxidized	0.0005	0.0770	0.9999
Cu-26%Cr	As-machined	0.0003	0.2854	0.8400
NiAl (second run)	As-machined	–0.000001	0.4002	0.0016

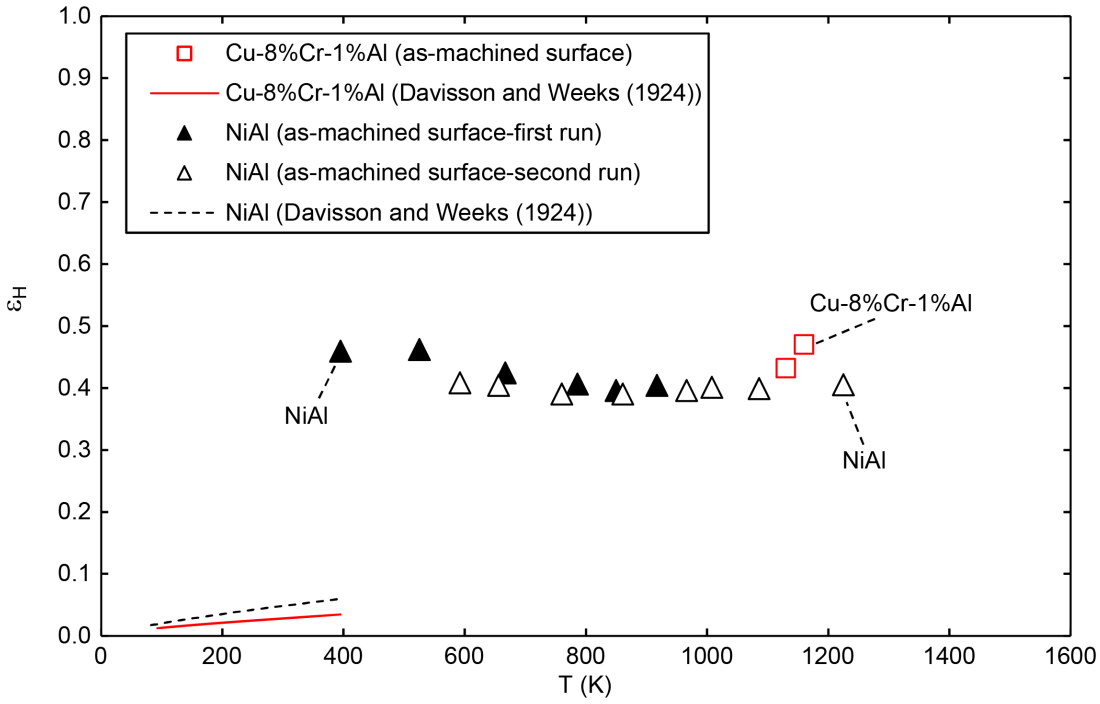

Figure 13.—Comparison of the predicted values of ε_H by the Davisson-Weeks model (Ref. 55) (Eq. (14)) with the experimental data for VPS Cu-8%Cr-1%Al and VPS NiAl (V2-03-166).

In contrast, ε_H was not significantly dependent on absolute temperature for the NiAl coating with $\varepsilon_H \sim 0.4$ between 395 and 1225 K. Since NiAl forms an Al_2O_3 surface layer, it is worth noting that a constant value of $\varepsilon_H \sim 0.4$ between 590 and 810 K was reported for oxidized Al specimens (Ref. 45). The magnitudes of ε_H for electropolished Al increased from about 0.01 at about 150 K to about 0.04 at about 750 K (Ref. 43).

The Davisson and Weeks (DW) model (Ref. 55) predicted that ε_H in metals is related to electrical resistivity through Equation (14).

$$\varepsilon_H = 0.751 * (\rho T)^{0.5} - 0.632 * (\rho T) + 0.670 * (\rho T)^{1.5} - 0.607 * (\rho T)^2 \quad (14)$$

Figure 13 compares the predicted values of ε_H from Equation (14) with the experimental data determined for Cu-8%Cr-1%Al and NiAl with as-machined surfaces. As is evident from Figure 13, the predictions of the DW model (Ref. 55) do not agree with the experimental data, where the predicted values are much

lower the experimental data by more than a factor of seven. Presumably, this difference may be due to the fact that the DW model assumes a pristine metallic surface and does not account for the progressive oxidation of the alloy at high temperatures.

4.0 Summary and Conclusions

This paper reports the temperature dependencies of electrical and thermal conductivities, thermal diffusivities and total hemispherical emissivities between 77 and 1200 K for several VPS or CS copper alloy, NiCrAlY and NiAl monolithic coatings. Data are also presented for extruded GRCop-84 and an as-cast Cu-17%Cr-5%Al. In general, the thermal conductivities of GRCop-84, Cu-8%Cr and Cu-26%Cr tend to decrease with increasing temperature although this trend was only observed above 673 K for the GRCop-84 alloy. In contrast, the thermal conductivities of the Cu-Cr-Al, NiCrAlY and NiAl coatings increased with increasing temperature. As expected, the presence of porosity in the VPS Cu-26%Cr and NiCrAlY coatings decreased the thermal conductivities of these coatings, where the thermal conductivity of the NiCrAlY coating was sensitive to porosity only above 973 K. The magnitudes of the thermal conductivity for extruded GRCop-84 and VPS NiCrAlY reported in the present investigation were larger than those reported in the literature. The electrical resistivity increased with increasing temperature for the VPS Cu-8%Cr-1%Al, CS Cu-23%Cr-5%Al and VPS NiAl coatings. It is demonstrated that the electrical resistivity data for the three coatings are best represented by a third order polynomial equation. Although the Wiedemann-Franz law was a reasonable fit for the $\lambda/\sigma_e - T$ data and the experimentally determined Lorenz numbers compared reasonably well with values reported in the literature, it is demonstrated that the Smith-Palmer equation was a better fit to the data. The magnitudes of ε_H increased linearly with increasing temperature for the VPS Cu-8%Cr and Cu-26%Cr coatings but it was essentially independent of temperature for VPS NiAl. It was observed that ε_H increased with the degree of oxidation consistent with the observations in the literature for oxidized Cu.

References

1. R.J. Quentmeyer, Experimental Fatigue Life Investigation of Cylindrical Thrust Chambers, NASA TM X-73665, 1977, NASA Lewis Research Center, Cleveland, OH.
2. D.K. Huzel and D.H. Huang, Modern Engineering for Design of Liquid-Propellant Rocket Engines, *Progress in Astronautics and Aeronautics*, (ed. A.R. Seebass), 1992, p. 67-134, American Institute of Aeronautics and Astronautics, Inc., Washington, DC.
3. J. Singh, G. Jerman, B. Bhat and R. Poorman, Microstructural Stability of Wrought, Laser and Electron Beam Glazed NARloy-Z Alloy at Elevated Temperatures, NASA TM-108431, 1993, NASA Marshall Space Flight Center, Huntsville, AL.
4. H.J. Kasper, Thrust Chamber Life Prediction, *Advanced High Pressure O_2/H_2 Technology*, NASA CP 2372 (eds. S.F. Morea and S.T. Wu), 1985, p. 36-43, NASA Marshall Space Flight Center, Huntsville, AL.
5. R.J. Quentmeyer, Rocket Thrust Chamber Thermal Barrier Coatings, *Advanced High Pressure O_2/H_2 Technology*, NASA CP 2372 (eds. S.F. Morea and S.T. Wu), 1985, p. 49-58, NASA Marshall Space Flight Center, Huntsville, AL.
6. D.B. Morgan and A.C. Kobayashi, Main Combustion Chamber and Cooling Technology Study – Final Report, NASA CR–184345, 1989, NASA Marshall Space Flight Center, Huntsville, AL.

7. D. Ellis and D. Keller, Thermophysical Properties of GRCop-84, NASA/CR—2000-210055, 2000, NASA Glenn Research Center, Cleveland, OH.
8. R. Holmes, D. Ellis and T. McKechnie, Robust Low Cost Aerospike/RLV Combustion Chamber by Advanced Vacuum Plasma Process, *Countdown to the Millennium Proceedings*, 36th Space Congress, 1999, Canaveral Council of Technical Societies, Cape Canaveral, FL.
9. R. Hickman, T. McKechnie and R. Holmes, Material Properties of Vacuum Plasma Sprayed Cu-8Cr-4Nb for Liquid Rocket Engines, Paper No. AIAA 2001-3693, 37th AIAA/ASME/SAE/ASEE/Joint Propulsion Conference, Salt Lake City, UT, 2001, p. 1-9, American Institute of Aeronautics and Astronautics, Inc., Washington D.C.
10. K.T. Chiang, P.D. Krotz and J.L. Yuen, Blanching Resistant Cu-Cr Coating by Vacuum Plasma Spray, *Surf. Coat. Technol.*, 1995, **76**, p. 14-19.
11. K.T. Chiang and J.P. Ampaya, Oxidation Kinetics of Cu-30vol.%Cr Coating, *Surf. Coat. Technol.*, 1996, **78**, p. 243-247.
12. T.A. Wallace, R.K Clark and K.T. Chiang, Dynamic Oxidation Performance of NARloy-Z with Cu-30 volume percent Cr Coating, *J. Spacecraft Rockets*, 1998, **35**, p. 546-551.
13. S. Elam, R. Holmes, T. McKechnie, R. Hickman and T. Pickens, VPS GRCop-84 Chamber Liner Development Efforts, 52nd JANAF Propulsion Meeting/1st Liquid Propulsion Subcommittee Meeting, Las Vegas, Chemical Propulsion Information Agency, 2004, p. 1-10, The Johns Hopkins University, Baltimore, MD.
14. S.V. Raj, L.J. Ghosn, C. Robinson and D. Humphrey, High Heat Flux Exposures of Overlay NiCrAlY-Coated GRCop-84 Substrates, *Mater. Sci. Eng. A.*, 2007, **457**, p. 300-312.
15. T. Fiedler, T. Fedorova, J. Rösler and M. Bäker, Design of a Nickel-Based Bond-Coat Alloy for Thermal Barrier Coatings on Copper Substrates, *Metals*, 2014, **4**, p. 503-518.
16. T. Fiedler, J. Rössler and M. Bäker, Development of a CuNiCrAl Bond Coat for Thermal Barrier Coatings in Rocket Combustion Chambers, *J. Thermal Spray Tech.*, 2015, **24**, p. 1480-1486.
17. S.V. Raj, C. Barrett, J. Karthikeyan and R. Garlick, Cyclic Oxidation Behavior of Cold-Sprayed CuCrAl-Coated and Uncoated GRCop-84 Substrates for Space Launch Vehicles, *Surf. Coat. Tech.*, 2007, **201**, p. 7222-7234.
18. P. Jain, S.V. Raj and K.J. Hemker, Characterization of NiCrAlY Coatings for a High Strength, High Conductivity GRCop-84 Copper Alloy, *Acta Materialia*, 2007, **55**, p. 5103-5113.
19. J.A. Nesbitt, S.V. Raj and L.A. Greenbauer-Seng, Overlay Coatings Technology Development for GRCop-84 Combustion Chamber Liners for Reusable Launch Vehicles, April 23-26, 2007, Paper No. AIAA-2007-2068, 48th AIAA/ASME/ASCE/AHS/ASC Structures, Structural Dynamics and Materials Conference, Honolulu, HI.
20. S.V. Raj, Comparison of the Isothermal Oxidation Behavior of As-Cast Cu-17%Cr and Cu-17%Cr-5%Al Part I: Oxidation Kinetics, *Oxidation of Metals*, 2008, **70**, p. 85-102.
21. S.V. Raj, Comparison of the Isothermal Oxidation Behavior of As-Cast Cu-17%Cr and Cu-17%Cr-5%Al Part II: Scale Microstructures, *Oxidation of Metals*, 2008, **70**, p. 103-119.
22. P.A. Siemers and R.L. Mehan, Mechanical and Physical Properties of Plasma Sprayed Stabilized Zirconia, Report No. 83CRD149, 1983, General Electric Company, Schenectady, NY.
23. W.J. Brindley, Properties of Plasma-Sprayed Bond Coats, *J. Thermal Spray Technology*, 1997, **6**, p. 85-90.

24. R.R. Holmes and T.N. McKechnie, Vacuum Application of Thermal Barrier Plasma Coatings, *Advanced Earth-to-Orbit Propulsion Technology*, 1988, **vol. 1**, p. 692-702, NASA CP 3012, NASA Marshall Space Flight Center, Huntsville, AL.
25. R.R. Holmes and T.N. McKechnie, Vacuum Plasma Spray Coating, *Application of Advanced Material for Turbomachinery and Rocket Propulsion*, AGARD CP-449, AD-A214-462, 1989, p. 17-1 to 17-5, North Atlantic Treaty Organization, Advisory Group for Aerospace Research and Development, Neuilly Sur Seine, France.
26. L. Pawlowski, *The Science and Engineering of Thermal Spray Coatings*, 2008, 2nd ed., John Wiley, Chichester, West Sussex, England.
27. D. Hanson and C.E. Rodgers, The Thermal Conductivity of Some Non-Ferrous Alloys, *J. Inst. Metals*, 1932, **48**, p. 37-45.
28. C.S. Smith and E.W. Palmer, Thermal and Electrical Conductivities of Copper Alloys, Tech. Pub. 648, *Trans. AIMME*, 1935, **117**, p. 225-245.
29. R.E.B. Makinson, The Thermal Conductivity of Metals, *Proc. Cambridge Phil Soc.*, 1938, **34**, p. 474-497.
30. C.C. Bidwell, Thermal Conductivity of Metals, *Phys. Rev.*, 1940, **58**, p. 561-564.
31. P.G. Klemens and R.K. Williams, Thermal Conductivity of Metals and Alloys, *Intern. Met. Rev.*, 1986, **31**, p. 197-215.
32. L. Weber and R. Tavangar, On the Influence of Active Element Content on Thermal Conductivity and Thermal Expansion of Cu-X (X =Cr,B) Diamond Composites, *Scripta Mater.*, 2007, **57**, p. 988-991.
33. S.V. Raj and A. Palczer, Thermal Expansion of Vacuum Plasma Sprayed Coatings, *Mater. Sci. Eng. A*, 2010, **A 527**, p. 2129-2135.
34. S.V. Raj, R. Pawlik and W. Loewenthal, Young's Moduli of Cold and Vacuum Plasma Sprayed Metallic Coatings, *Mater. Sci. Eng. A*, 2009, **A 513-514**, 59-63.
35. J. Karthikeyan, Development of Oxidation Resistant Coatings on GRCop-84 Substrates by Cold Spray Process, NASA/CR—2007-214706, 2007, NASA Glenn Research Center, Cleveland, OH.
36. Thermophysical Properties Research Laboratory, Inc., http://www.tprl.com/services.html.
37. ASTM Standard E1461, Standard Test Method for Thermal Diffusivity by the Flash Method, ASTM Annual Book of Standard, 2004, **vol. 14.02**, ASTM International, West Conshohocken, PA.
38. S.V. Raj, Thermophysical Properties of Cold and Vacuum Plasma Sprayed Cu-Cr Alloys, NiAl and NiCrAlY Coatings Part II: Specific Heat Capacity, *J. Eng. Mater. Perform.*, 2017, **vol. 26**, **11**, p. 5456-5471. https://link.springer.com/article/10.1007/s11665-017-3015-x; NASA/TM—2017-219716.
39. D. Zhu and R.A. Miller, Thermal Conductivity and Elastic Modulus Evolution of Thermal Barrier Coatings under High Heat Flux Conditions, *J. Therm. Spray Tech.*, 2009, **9**, p. 175-180.
40. ASTM C835-06, Standard Test Method for Total Hemispherical Emittance of Surfaces up to 1400ºC, *ASTM Annual Book of Standards*, **vol. 04.06**, *ASTM International*, West Conshohocken, PA.
41. W.S. Walston and R. Darolia, Effect of Alloying on Physical Properties of NiAl, *High-Temperature Ordered Intermetallic Alloys V*, (eds. I. Baker, R. Darolia, J.D. Whittenberger and M.H. Yoo, 1993, **vol. 288**, p. 237-242, *MRS Symposium Proceedings*, Materials Research Society, Pittsburgh, PA.
42. C.A. Wert and R.M. Thomson, *Physics of Solids (2nd ed.)*, 1970, McGraw-Hill, New York, NY.
43. K.G. Ramanathan, S.H. Yen and E.A. Estalote, Total Hemispherical Emissivities of Copper, Aluminum, and Silver, *Appl. Opt.*, 1977, **16**, p. 2810-2817.

44. P.J. Klemens, Deviations from Matthiessens' Rule and Lattice Thermal Conductivity of Alloys, *Australian Journal of Physics*, 1959, **12**, p.199-202.
45. W.R. Wade, Measurements of Total Hemispherical Emissivity of Various Oxidized Metals at High Temperature, NACA TN 4206, 1958, National Advisory Committee for Aeronautics, Washington D.C.
46. R.A. Matula, Electrical Resistivity of Copper, Gold, Palladium and Silver, *J. Phys. Chem. Ref. Data*, 1979, **8**, p. 1147-1298.
47. C. Kittel, *Introduction to Solid State Physics* (4th ed.), 1971, Wiley, New York, NY.
48. P.D. Desai, H. M. James and C. Y. Ho, Electrical Resistivity of Aluminum and Manganese, *J. Phys. Chem. Ref. Data*, 1984, **13**, p. 1131-1172.
49. J-P. Poirier, *Introduction to the Physics of the Earth's Interior* (2nd ed.), Cambridge University Press, Cambridge, UK (1991).
50. C. Uher, Thermal Conductivity of Metals, *Thermal Conductivity: Theory, Properties, and Applications* (ed. T.M. Tritt), 2004, p. 21-91, Springer, New York, NY.
51. N.F. Mott and H. Jones, The Theory of the Properties of Metals and Alloys, 1958, Dover, N.Y., NY.
52. J.H. Dellinger, The Temperature Coefficient of Resistance of Copper, *Bull. Bur. Stds.*, 1911, **7**, p. 71-101.
53. L. Weiner, P. Chiotti and H.A. Wilhem, Temperature Dependence Of Electrical Resistivity of Metals, *Ames Laboratory ISC Technical Reports, Paper 58*, 1952, United States Atomic Energy Commission, Oak Ridge, TN. http://lib.dr.iastate.edu/ameslab_iscreports/58.
54. A. Bid, A. Bora and A. K. Raychaudhuri, Temperature Dependence of the Resistance of Metallic Nanowires (diameter ≥ 15 nm): Applicability of Bloch-Grüneisen Theorem, *Phys. Rev. B*, 2006, **74**, 035426.
55. C. Davisson and J. R. Weeks, The Relaxation between the Total Thermal Emissive Power of a Metal and its Electrical Resistivity, *J. Opt. Soc. Amer. Rev. Sci. Instrum.*, 1924, **8**, p. 581-605.